

Ultrafast Stiffening of the Lattice Potential and Metastable State Formation in 1T-TiSe₂

Xue-Qing Ye,¹ Hao Liu,¹ Qi-Yi Wu,¹ Chen Zhang,¹ Xiao-Fang Tang,² Bo Chen,¹
Chuan-Cun Shu,¹ Hai-Yun Liu,³ Yu-Xia Duan,¹ Peter M. Oppeneer,⁴ and Jian-Qiao Meng^{1,*}

¹*School of Physics, Central South University, Changsha 410083, China*

²*Department of Physics and Electronic Science, Hunan University of Science and Technology, Xiangtan 411201, Hunan, China*

³*Beijing Academy of Quantum Information Sciences, Beijing 100085, China*

⁴*Department of Physics and Astronomy, Uppsala University, Box 516, S-75120 Uppsala, Sweden*

(Dated: Wednesday 3rd December, 2025)

We use ultrafast optical spectroscopy to investigate the electronic and lattice dynamics of the charge-density wave (CDW) material 1T-TiSe₂ across various temperatures and pump fluences. We reveal a close relationship between the observed ultrafast dynamical processes and two characteristic temperatures: T_{CDW} (~ 202 K) and T^* (~ 165 K). Two coherent phonon modes are identified: a high-frequency A_{1g} mode (ω_1) and a lower-frequency A_{1g} CDW amplitude mode (ω_2). In stark contrast to thermal melting, where phonons soften, the CDW amplitude mode exhibits anomalous hardening (frequency upshift) with increasing pump fluence. We establish this hardening as the direct signature of an ultrafast restoration of the bare lattice potential. The photoexcited carrier plasma screens the long-range electron-phonon interactions that drive the Peierls-like instability, effectively “undressing” the soft phonon and driving its frequency toward the stiffer value of the unrenormalized lattice. Furthermore, an abrupt increase in the excited state buildup time above a critical pump fluence marks a sharp boundary to a photoinduced metastable metallic state. These findings demonstrate that the CDW order in 1T-TiSe₂ is governed by a fragile, fluence-tunable competition between excitonic correlations and lattice dynamics.

Layered transition metal dichalcogenides (TMDCs), with the general formula MX_2 (M = transition metal, X = chalcogenide), are a prominent class of two-dimensional (2D) materials. Their diverse properties, including superconductivity [1–3] and charge density waves (CDW) [4, 5], arise from complex interactions among charge, lattice, spin, and orbital degrees of freedom. This makes TMDCs an excellent platform for investigating correlated electronic systems. Among them, 1T-TiSe₂ is particularly notable as a semimetal with a small band overlap that undergoes a $2 \times 2 \times 2$ commensurate CDW transition near 202 K (T_{CDW}), accompanied by significant lattice and electronic structural reshaping.

1T-TiSe₂ exhibits a rich variety of physical phenomena, including CDW formation [6], chiral CDW states [7], and potential excitonic Bose-Einstein condensation [8], along with superconductivity under doping or pressure [9–12]. At room temperature, 1T-TiSe₂ is a semimetal, featuring a Se 4p hole pocket at the Γ point and Ti 3d electron pockets near the Brillouin zone’s M/K points, with an indirect band overlap of approximately 80 meV [Fig. 1(a)] [15–19]. Cooling below T_{CDW} induces a commensurate CDW phase with a $2 \times 2 \times 2$ periodic lattice distortion [6]. This transition leads to exciton insulator behavior, characterized by band folding and partial gap opening at the M/ T^* point, as shown in Fig. 1(b) [20, 21].

The precise origin of the CDW phase in 1T-TiSe₂ remains a subject of ongoing debate, with leading theories considering a combination of Peierls instability, Jahn-Teller effects, and, significantly, the condensation of excitons — bound electron-hole pairs [9, 21–26]. This last mechanism suggests 1T-TiSe₂ may realize an excitonic insulator. Further complexity arises below T_{CDW} , where a broad resistivity peak is observed around 165 K (T^*) [6, 19]. The origin of this T^* anomaly is also debated, with proposed explanations including quasiparticle effective mass renormalization [15], Fermi surface reconstruction [27], incoherence-to-coherence crossover [28],

and a shift in dominant carrier type [29]. Ultrafast optical spectroscopy, with its ability to probe dynamics on femtosecond timescales, offers a powerful approach to elucidate these competing interactions and reveal the underlying mechanisms [30].

In this Letter, we present a comprehensive ultrafast optical spectroscopy investigation of 1T-TiSe₂ that uniquely resolves the intricate interplay between its electronic and lattice dynamics. We precisely map how quasiparticle dynamics correlate with the known T_{CDW} and T^* (~ 165 K) phases, observing distinct changes in carrier relaxation pathways, including a notable sign change in a relaxation component below T^* . Our measurements further identify two coherent phonon modes: the high-frequency A_{1g} mode and, critically, the A_{1g} -CDW amplitude mode. We demonstrate that the A_{1g} -CDW amplitude mode (ω_2) exhibits unexpected hardening under increasing pump fluence. This behavior is striking because ω_2 is the soft mode of the transition; thermally suppressing the CDW order typically softens this mode. Our observa-

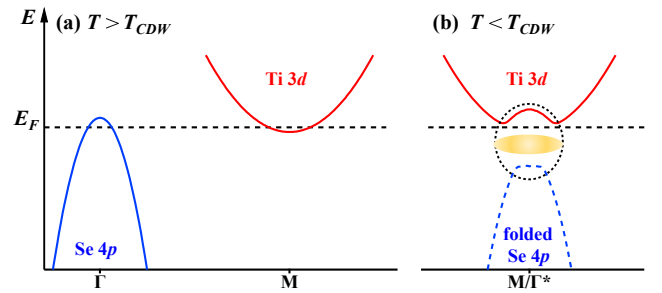


FIG. 1. (a) Electronic structure of 1T-TiSe₂ along Γ -M in the normal state ($T > T_{\text{CDW}}$). (b) Band structure near M/ T^* in the CDW state ($T < T_{\text{CDW}}$), illustrating band folding and the subsequent hybridization between the folded Se 4p and Ti 3d bands, leading to the formation of excitonic correlations between electron-hole pairs.

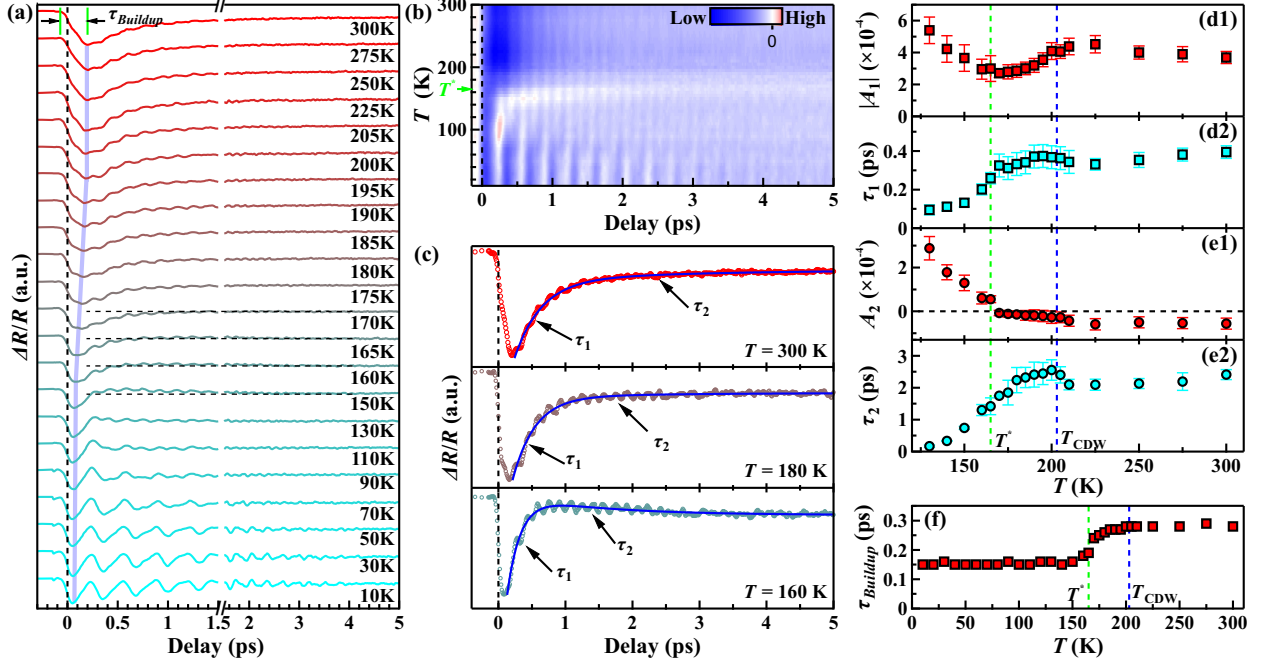


FIG. 2. **Temperature-dependent ultrafast reflectivity dynamics of 1T-TiSe₂.** (a) Transient $\Delta R/R$ vs. delay time over temperatures ranging from 10 to 300 K at a pump fluence of $\sim 40 \mu\text{J}/\text{cm}^2$. Note the break in the x axis. (b) 2D pseudocolor map of $\Delta R/R$ as a function of delay time and temperature. (c) Bi-exponential fits (blue lines) to $\Delta R/R$ at selected temperatures. Arrows indicate the initial (τ_1) and second (τ_2) relaxation processes. (d1, d2) Amplitude ($|A_1|$) and lifetime (τ_1) of the initial relaxation as a function of temperature. (e1, e2) Amplitude (A_2) and lifetime (τ_2) of the second relaxation as a function of temperature. (f) Temperature dependence of buildup time (τ_{Buildup}) as defined in (a). The vertical blue and green dashed lines indicate T_{CDW} and T^* , respectively.

tion of hardening implies a rapid reconfiguration of the interatomic potential energy surface. It suggests that the dense photoexcited population suppresses the electronic renormalization responsible for the lattice instability, thereby decoupling the lattice from the CDW correlations and driving the phonon frequency toward the stiffer value of the unrenormalized state. Moreover, an abrupt increase in the excited state buildup time at a critical fluence, together with the results from short-time Fourier transform analysis, definitively indicates photoinduced quenching of the CDW order and transition to a transient metastable state. These findings underscore the profound, dynamic role of electron-phonon coupling in 1T-TiSe₂'s charge-density wave transition.

was conducted using a noncollinear pump-probe setup driven by a Yb-based femtosecond laser (1 MHz). The output seeded an optical parametric amplifier and compressor, generating ~ 35 fs pulses centered at 800 nm (1.55 eV) with a bandwidth of ~ 35 nm [31, 32]. Orthogonally polarized pump ($\sim 80 \mu\text{m}$ spot) and probe ($\sim 40 \mu\text{m}$ spot) beams were focused onto freshly cleaved 1T-TiSe₂ single crystals, grown by chemical vapor transport with iodine [33]. Experiments were performed under high vacuum (10^{-6} Torr) across a temperature range of 4 – 300 K.

Figure 2(a) presents the transient reflectivity ($\Delta R/R$) of 1T-TiSe₂ from 10 to 300 K, measured at a low pump fluence ($40 \mu\text{J}/\text{cm}^2$), well below the critical fluence for quenching exciton condensation [14]. Photoexcitation elicits an instantaneous $\Delta R/R$ change followed by multiple recovery processes, indicating diverse relaxation pathways. A strong tempera-

ture dependence is evident, marked by pronounced oscillations throughout the entire range. The time to reach the initial $\Delta R/R$ minimum shifts to longer delays with increasing temperature (purple line), a behavior discussed further below.

As temperature decreases, the oscillations' amplitude and contribution significantly increase, dominating the low-temperature signal. The 2D pseudocolor map in Fig. 2(b) further illustrates this, revealing a robust, long-period oscillation at low temperatures. As shown in the time-domain data of Fig. 2(a), this oscillation exhibits a cosine-like form, a signature of a dispersive excitation. This mechanism involves the sudden modification of the ionic potential-energy surface following photoexcitation [34]. This long-period mode gradually damps and diminishes with increasing temperature, merging with a shorter-period oscillation around 130 K. Above 130 K, only weaker, shorter-period oscillations are resolvable up to 300 K. Notably, at high temperatures, the $\Delta R/R$ signal is entirely negative; however, below T^* (165 K), a positive signal emerges around 0.5 ps delay. This distinct temperature evolution of $\Delta R/R$ highlights its sensitivity to subtle electronic structure changes associated with T^* .

To quantitatively analyze the observed dynamics, we isolated the non-oscillatory component of the transient reflectivity. As shown by the solid blue lines in Fig. 2(c), this response is accurately described by a bi-exponential decay model: $\Delta R/R = A_1 e^{-t/\tau_1} + A_2 e^{-t/\tau_2} + C$. Here, A_i and τ_i represent the amplitude and relaxation time of the i -th component, while C accounts for long-lifetime processes. This fitting was applied to data after the initial $\Delta R/R$ minimum. The extracted

temperature dependence of amplitudes ($|A_1|$ and A_2) and relaxation times (τ_1 and τ_2) are presented in Figs. 2(d1) - 2(e2). Due to the dominance of oscillatory signals at low temperatures, our analysis focuses on $T \geq 130$ K, a range sufficient as no additional transitions are known below this temperature.

The temperature evolution of both amplitudes and relaxation times reveals two distinct anomalies, centered around T_{CDW} and T^* . At high temperatures (T_{CDW}), τ_1 slightly decreases with decreasing temperature, consistent with observations in other semimetallic materials like 1T-TiTe₂ [35], and WTe₂ [36]. Given its hundreds-of-femtoseconds timescale, τ_1 is primarily attributed to electron-phonon (*e-ph*) thermalization, representing the cooling of the hot electronic system through energy transfer to the lattice. Electron-electron (*e-e*) scattering, occurring on much faster timescales, is not the dominant process here. Following this initial thermalization, quasiparticles near the Fermi level undergo further decay. This second component, τ_2 , is likely associated with phonon-assisted *e-h* recombination between the conduction (Ti 3d) and (folded) valence (Se 4p) bands (Fig. 1(a)), a commonly observed process in semimetallic systems [35, 36].

As temperature approaches T_{CDW} from above, both τ_1 and τ_2 show a modest increase, signaling the influence of electronic structure modifications due to the impending CDW formation. Upon further cooling below T_{CDW} , both amplitudes ($|A_1|$ and $|A_2|$) and lifetimes (τ_1 and τ_2) decrease with decreasing temperature. A more dramatic change occurs when cooling across T^* . Below T^* , $|A_1|$ increases with decreasing temperature, while τ_1 simultaneously decreases at an accelerated rate. Concurrently, τ_2 continues to decrease, with its rate of reduction slightly increasing as temperature drops. Notably, A_2 undergoes a sign change from a small negative to a positive value and rapidly increases in magnitude with further cooling. This profound sign change in $|A_2|$ strongly indicates a significant modification in the underlying electronic structure and/or relaxation pathways.

To elucidate the distinct temperature-dependent behavior around T^* , we propose two possible mechanisms. First, a change in recombination dynamics may be responsible. Above T^* , recombination could primarily involve free *e-h* pairs. However, below T^* , the increasing prominence of excitonic correlations or the formation of collective CDW states might significantly alter these recombination pathways. This aligns with previous ARPES studies on 1T-TiSe₂ reporting an incoherence-to-coherence crossover at 165 K [28], attributed to potential exciton condensation below the primary CDW transition. Exciton-assisted recombination can produce an optical response with an opposite sign to that of free-carrier recombination, because excitons interact differently with the probe light: instead of contributing to absorption through free-carrier transitions, bound *e-h* pairs modify the dielectric function via their discrete resonance states and altered selection rules. Second, a shift in the dominant carrier type could contribute. A downshift of the Ti 3d band around 165 K has been observed, leading to a transition from hole-like to electron-like dominant carriers with decreasing temperature [29]. Such a change in carrier majority could manifest as a sign change in

the $\Delta R/R$ signal, as optical response is sensitive to the density of states and effective mass of the involved carriers.

We next analyze the excited state buildup time, τ_{Buildup} , another notable temperature-dependent quantity. Given the strong oscillatory signals in $\Delta R/R$ at low temperatures (Figs. 2(a) and 2(b)), standard fitting methods for τ_{Buildup} are challenging [32, 37]. We therefore define τ_{Buildup} as the interval from the onset of reflectivity change until the signal reaches its minimum, as schematically shown in Fig. 2(a). This definition does not account for instrumental time resolution, implying the reported τ_{Buildup} will be slightly longer than the intrinsic excited state formation time. Figure 2(f) shows the temperature dependence of τ_{Buildup} . Above T_{CDW} , τ_{Buildup} remains approximately constant at ~ 0.3 ps. As temperature decreases below T_{CDW} , τ_{Buildup} decreases, settling at a new, approximately constant value of ~ 0.15 ps slightly below T^* . The observed ~ 0.3 ps buildup time in the normal state is significantly longer than typical values in other semimetallic materials [35, 36]. This suggests that initial excited state formation in 1T-TiTe₂ involves mechanisms beyond simple electronic transitions, distinguishing it from conventional semimetals.

At low temperatures ($T < T^*$), the ~ 0.15 ps excited state buildup time is comparable to the timescale for CDW gap reduction (quenching) observed in Tr-ARPES measurements at low pump fluence [37–39]. This correlation strongly suggests that carrier multiplication via impact ionization, specifically interband scattering between the Ti 3d and Se 4p bands, significantly influences τ_{Buildup} in the low-temperature CDW phase [38]. As temperature increases above T^* , the CDW gap continues to decrease and the Ti 3d band shifts upward in energy. This expands the phase space for *e-e* interband scattering, prolonging carrier accumulation near the Fermi level and consequently extending τ_{Buildup} . When temperature exceeds T_{CDW} , the CDW gap closes, and the characteristic band folding vanishes. In this normal state, optical excitation directly promotes electrons from the Ti 3d-derived valence band to the conduction band around the Γ point. These hot electrons rapidly scatter away from Γ and accumulate at the M point within the conduction band. The timescale for these interband scattering and accumulation processes aligns well with the ~ 0.3 ps τ_{Buildup} observed in the normal state by Tr-ARPES [34].

Having analyzed the non-oscillatory response, we now turn to the significant oscillatory component of the $\Delta R/R$ signal. These oscillations are indicative of collective bosonic excitations and serve as a reliable measure of phase transitions [40, 41]. Prominent high-frequency oscillations appear instantaneously upon photoexcitation, superimposed on the $\Delta R/R$ profile (Figs. 2(a) and 2(b)). The time-domain oscillations, isolated by subtracting the non-oscillatory decay, are presented in Fig. 3(a) for several selected temperatures. As temperature increases, the oscillation amplitudes decrease, and a clear beating behavior emerges. This beating confirms the presence of multiple coexisting bosonic collective excitation modes.

To investigate these bosonic properties, we performed a Fast Fourier Transform (FFT) analysis on the oscillatory data.

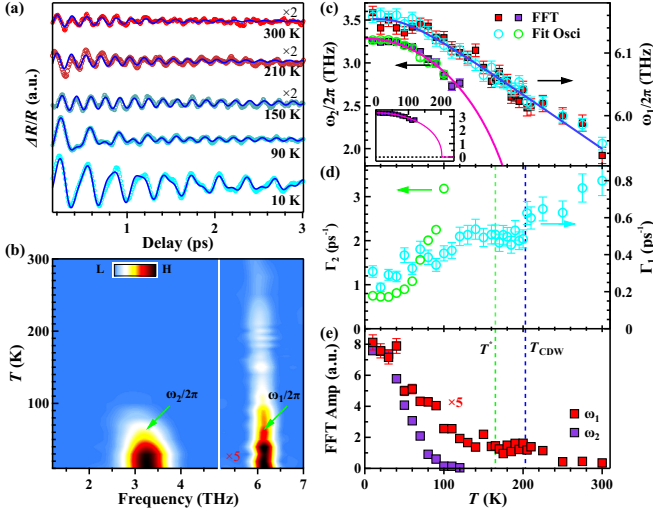


FIG. 3. **Oscillatory part of temperature-dependent data** (a) Oscillations from the transient reflectivity at five selected temperatures, with blue lines represent fits using Eq. (1). (b) False-color FFT spectrum as a function of frequency and temperature. (c) Temperature dependence of $\omega_1/2\pi$ and $\omega_2/2\pi$ from the FFT (squares) and fits (circles). The solid magenta lines is a fit to the frequency ω_2 with a mean-field-like as described in the text. (d) Temperature dependence of damping rates Γ_1 and Γ_2 from fits. The solid cyan lines in (c) and (d) are anharmonic phonon model fit to data obtained from fitting to Eq. (1). (e) Temperature dependence of FFT amplitudes of ω_1 and ω_2 .

Figure 3(b) presents the FFT spectrum as a function of frequency and temperature. At low temperatures, two distinct terahertz modes, ω_1 and ω_2 , were observed. At 10 K, their frequencies were 6.16 THz (25.5 meV or 205.5 cm^{-1}) and 3.26 THz (13.5 meV or 108.7 cm^{-1}), respectively. As temperature increases, the amplitudes of both modes decrease rapidly, with ω_2 becoming difficult to resolve above 120 K. The higher frequency mode, ω_1 , corresponds to coherent A_{1g} phonons [33, 42] and persists up to room temperature. Conversely, the lower frequency mode, ω_2 , is attributed to a photoinduced coherent A_{1g} -CDW phonon [14, 22, 26, 43]. This mode is a direct consequence of the periodic lattice distortion (PLD) and is absent in the normal state. The extracted frequencies and FFT amplitudes for both modes are summarized in Figs. 3(c) and 3(e) (squares).

Phonon properties were also extracted by fitting the damped oscillations using the following expression [blue solid lines in Fig. 3(a)]:

$$\left(\frac{\Delta R}{R}\right)_{osc} = \sum_{i=1,2} A_i e^{-\Gamma_i t} \sin(\omega_i t + \phi_i), \quad (1)$$

where A_i , Γ_i , ω_i , and ϕ_i are the amplitude, damping rate, frequency, and initial phase of the i -th oscillatory signal, respectively. The extracted temperature dependence of ω_1 and ω_2 is plotted in Fig. 3(c) (circles), and damping rates Γ_1 and Γ_2 in Fig. 3(d) (circles). All parameters exhibit significant variations with temperature. Specifically, both ω_1 and ω_2 soften (redshift) as temperature increases. While ω_1 is well-described by optical phonon anharmonic effects [44, 45]

within our experimental resolution, Γ_1 cannot be fitted by anharmonic effects across the entire temperature range, showing anomalous behavior around T_{CDW} and T^* . As depicted in Fig. 3(e), the FFT amplitude of the ω_1 mode also displays a significant anomaly around T_{CDW} and T^* . These observations indicate a strong, previously unreported relationship between ω_1 and both the CDW transition and T^* .

The frequency of A_{1g} -CDW phonon mode (ω_2) becomes challenging to determine accurately at high temperatures due to its rapidly increasing damping rate and decreasing amplitude with rising temperature (see section I in the Supplemental Material [46]). The lower frequency mode, ω_2 , clearly exhibits characteristics of a CDW amplitude mode. First, its temperature dependence can be described by a mean-field-like relationship [47, 48]: $\omega_2 = \omega_2(0) \times (1 - T/T_{CDW})^\beta$. Here, we choose $\beta = 0.22$, a value deviating from the mean-field theory prediction of $\beta = 0.5$, to align with the bulk sample's $T_{CDW} = 202$ K. Second, the intensity of ω_2 mode diminishes as the CDW lattice loses coherence when the temperature approaches T_{CDW} .

The established interplay among low free carrier density, poor Coulomb screening, and exciton condensation in 1T-TiSe₂ offers a crucial platform to experimentally verify the electronic origin of its CDW. This can be achieved by modulating the ordered state through photoexcitation, as introducing excess carriers enhances Coulomb scattering, potentially disrupting the coherent exciton state and suppressing the ordered phase. To explore these photoinduced transient phase transitions [49], we conducted a systematic study of the fluence-dependent ultrafast dynamics.

Figure 4(a) presents the transient differential reflectivity ($\Delta R/R$) as a function of pump-probe delay for various pump fluences (from $\sim 30 \mu\text{J}/\text{cm}^2$ to $\sim 280 \mu\text{J}/\text{cm}^2$) at 4 K. The $\Delta R/R$ response exhibits notable variations, particularly an abrupt increase in the excited state buildup time ($\tau_{Buildup}$) above a critical fluence (F_c) of $\sim 140 \mu\text{J}/\text{cm}^2$. This critical fluence aligns with previous reports concerning CDW order quenching [39]. The complex interplay of photoinduced effects is further visualized in the 2D pseudocolor map of $\Delta R/R$ in Fig. 4(b), which spans pump-probe delay and fluence. This map clearly reveals multiple distinct oscillatory features, all exhibiting strong fluence dependence. To quantitatively characterize these oscillations, Fourier analysis was employed. Figure 4(c) displays the FFT spectrum as a function of frequency and fluence, clearly highlighting two prominent phonon modes, ω_1 and ω_2 .

Figures 4(d1) and 4(d2) display the fluence dependence of the frequency and FFT amplitude of ω_1 at various temperatures. As expected [35], the frequency of ω_1 generally decreases with increasing pump fluence, indicative of photoinduced softening. Notably, this decrease is significantly more pronounced below T_{CDW} than in the normal state. The amplitude of ω_1 generally increases with increasing fluence; however, at 4 K and 40 K, the amplitude exhibits anomalous behavior above $\sim 160 \mu\text{J}/\text{cm}^2$ and $\sim 120 \mu\text{J}/\text{cm}^2$, respectively, before continuing to increase with further fluence increments.

Figures 4(e1) and 4(e2) show the fluence dependence of

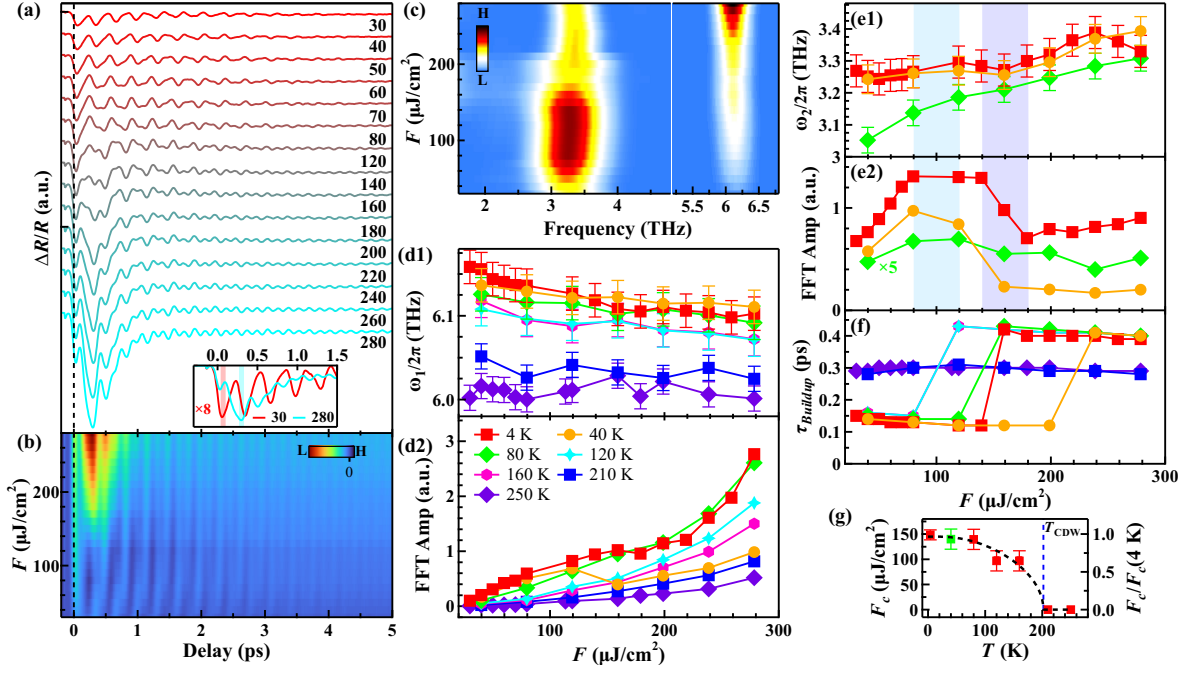


FIG. 4. **Pump fluence-dependent ultrafast dynamics of 1T-TiSe₂.** (a) Transient $\Delta R/R$ as a function of delay time for various pump fluences at 4 K. (b) 2D pseudocolor map of $\Delta R/R$ as a function of delay time and pump fluence. (c) False-color FFT spectrum as a function of frequency and pump fluence. (d1,d2) Fluence dependence of ω_1 frequency and FFT amplitude at different temperatures. (e1, e2) Fluence dependence of ω_2 frequency and FFT amplitude at different temperatures. (f) Fluence dependence of τ_{Buildup} for various temperatures. (g) Temperature dependence of critical fluence F_c . The dashed black line is a fit to the $F_c(T)$ using an empirical mean-field expression for a second-order phase transition, $F_c(T) \propto \tanh^2[\alpha\sqrt{T_{\text{CDW}}/T - 1}\Theta(T_{\text{CDW}} - T)]$ [50], where α is a fitting parameter and Θ is the Heaviside step function.

the frequency and amplitude of ω_2 at 4 K, 40 K, and 80 K. Surprisingly, unlike conventional materials [31, 35, 51], ω_2 's amplitude exhibits an abnormal increase in frequency (hardening) with increasing pump fluence. This hardening cannot be attributed to laser heating, as ω_2 is known to downshift with increasing temperature [Fig. 3(c)]. Specifically, at 80 K, ω_2 monotonically increases by approximately 8% as fluence rises from $\sim 30 \mu\text{J}/\text{cm}^2$ to $\sim 280 \mu\text{J}/\text{cm}^2$, with a rate twice as high as that observed at 4 K and 40 K. At 4 K, ω_2 frequency exhibits a more complex, non-monotonic behavior: it initially slowly increases, then decreases around $120 \mu\text{J}/\text{cm}^2$, and subsequently increases above $160 \mu\text{J}/\text{cm}^2$, before being suppressed above $240 \mu\text{J}/\text{cm}^2$. Similar anomalies in ω_2 frequency variation are observed around $160 \mu\text{J}/\text{cm}^2$ at 40 K. Concurrently, the amplitude of ω_2 at 4 K initially increases continuously, then remains almost unchanged above $80 \mu\text{J}/\text{cm}^2$, shows an anomalous decrease above $120 \mu\text{J}/\text{cm}^2$, and resumes its increase above $180 \mu\text{J}/\text{cm}^2$. At 80 K, the amplitude of ω_2 shows a weaker fluence dependence but is also suppressed under higher pump fluences.

To further characterize the unexpected frequency upshift of ω_2 , short-time Fourier transform (STFT) analysis was performed. This analysis strikingly reveals that the phonon frequency blueshift occurs immediately upon photoexcitation and recovers to near equilibrium within approximately 1 ps under high light fluence (see Fig. S2 of the Supplemental Material [46]). This observation indicates a dynamic stiffening of the phonon mode immediately following photoexcitation.

The hardening of the ω_2 amplitude mode provides a unique window into the microscopic forces stabilizing the CDW. In the equilibrium CDW state, ω_2 acts as the “soft mode,” its frequency significantly suppressed (renormalized) relative to the bare lattice frequency by strong e -ph coupling and excitonic correlations. Thermal excitations typically flatten the free-energy potential, further softening the mode. However, our observation of fluence-dependent hardening reveals a fundamentally non-thermal mechanism: the ultrafast recovery of the bare lattice potential.

We attribute this to the transient suppression of the electronic renormalization. The dense photoexcited e - h plasma efficiently screens the Coulomb interactions and the specific susceptibility peak that drives the CDW instability. With this electronic “drag” removed, the effective lattice potential steepens, and the phonon frequency blueshifts toward the stiffer value of the unrenormalized state. This process is not merely a “decoupling” [52] but a transient removal of the Peierls driving force. The fact that this hardening occurs on a sub-picosecond timescale (as shown by STFT analysis in section II in Supplementary Materials [46]) confirms that the electronic glue holding the CDW distortion is quenched faster than the lattice can thermally relax, effectively snapping the lattice potential back to its metallic stiffness. Furthermore, this observation aligns with Tr-ARPES and ultrafast electron diffraction measurements on 1T-TiSe₂, which indicate a photoinduced ultrafast structural phase transition and a transient metastable metallic state [39]. These combined in-

sights provide compelling evidence that strong ultrafast photoexcitations can not only completely quench the CDW order on a short timescale, but also induce a transition to a distinct metastable state, even when the lattice temperature remains well below T_{CDW} .

Supporting this picture of potential reconstruction, the excited state buildup time (τ_{Buildup}) exhibits a sharp transition that mirrors the phonon dynamics. As shown in Fig. 4(f), below T_{CDW} , τ_{Buildup} undergoes a step-like increase from ~ 0.15 ps to ~ 0.4 ps once the fluence exceeds a temperature-dependent critical value F_c (the detailed determination of the critical fluence at 40 K is provided in Section III of the Supplemental Material [46]). As summarized in Fig. 4(g), F_c decreases monotonically with increasing temperature and vanished near T_{CDW} . We attribute this behavior to the fact that F_c corresponds to the critical coherent phonon amplitude required to drive the system into the metastable state. With increasing temperature, thermal fluctuations lower the energy barrier separating the potential minima, thereby reducing the optical fluence needed to induce switching. This abrupt prolongation of the carrier relaxation signals the complete collapse of the CDW gap and entry into the photoinduced metastable metallic state previously identified in tr-ARPES and ultrafast electron diffraction (UED) studies [14, 39]. In the low-fluence CDW phase, the presence of the gap restricts the available phase space, and carrier multiplication via impact ionization dominates, giving rise to short buildup times. Above F_c , the quenching of the CDW order closes the gap and restores the metallic Fermi surface. The resulting increase of τ_{Buildup} to values exceeding even the normal-state average suggests the emergence of a distinct metastable population, likely stabilized by the modified lattice potential indicated by the hardening of ω_2 . Importantly, our results bridge a key gap between previous electronic and structural probes. While UED directly observed the structural transition to a metastable state, it could not track changes in the stiffness of the underlying potential. Here, the coincidence between amplitude-mode hardening and F_c demonstrates that this metastable state is characterized by a transiently stiffened—or“bare”—interatomic potential liberated from CDW-induced softening. Thus, the photoinduced transition in 1T-TiSe₂ is not a simple melting of the CDW phase but a deterministic switching into a state in which lattice rigidity is momentarily restored through plasma screening.

In conclusion, ultrafast optical measurements reveal that 1T-TiSe₂ can be driven nonthermally across a sharp, fluence-dependent boundary into a metastable metallic state. The transition is signaled by a reproducible critical fluence, an abrupt lengthening of the excited-state buildup time, and—most strikingly—a sub-ps hardening of the A_{1g} -CDW amplitude mode (ω_2). Since this mode manifests only within the CDW phase, its frequency increase serves as a direct signature of lattice potential stiffening, resulting from the disruption of the electron-phonon renormalization by the photoexcited plasma. The coincidence of these effects ties the enigmatic T^* crossover to an excitonic-dominated recombination channel that is highly susceptible to photoinduced screening.

These observations establish a unified picture in which excitonic correlations and dynamic electron-phonon coupling compete on ultrafast timescales, enabling controlled, nonthermal reconfiguration of collective order in a prototypical CDW material.

This work was supported by the National Key Research and Development Program of China (Grant No. 2022YFA1604204), the Beijing National Laboratory for Condensed Matter Physics (No. 2024BNLCMPKF001), the National Natural Science Foundation of China (Grant No. 12074436), and the Science and Technology Innovation Program of Hunan Province (Grant No. 2022RC3068). P. M. O. acknowledges funding from the K. and A. Wallenberg Foundation (Grants No. 2022.0079 and No. 2023.0336) and from the Swedish Research Council (VR) (Grant No. 2022-06725).

* Corresponding author: jqmeng@csu.edu.cn

- [1] H. Noh, J. Jeong, E. Cho, K. Kim, B. I. Min, and B. Park, Experimental Realization of Type-II Dirac Fermions in a PdTe₂ Superconductor, *Phys. Rev. Lett.* **119**, 016401 (2017).
- [2] S. Manzeli, D. Ovchinnikov, D. Pasquier, O. V. Yazyev, and A. Kis, 2D transition metal dichalcogenides, *Nat. Rev. Mater.* **2**, 17033 (2017).
- [3] A. Jindal, A. Saha, Z. Li, T. Taniguchi, K. Watanabe, J. C. Hone, T. Birol, R. M. Fernandes, C. R. Dean, A. N. Pasupathy, and D. A. Rhodes, Coupled ferroelectricity and superconductivity in bilayer T_d -Mo₂, *Nature* **613**, 48 (2023).
- [4] K. Rossnagel, On the origin of charge-density waves in select layered transition-metal dichalcogenides, *J. Phys.: Condens. Matter* **23**, 213001 (2011).
- [5] J. Hwang, W. Ruan, Y. Chen, S. Tang, M. F. Crommie, Z. Shen, and S. Mo, Charge density waves in two-dimensional transition metal dichalcogenides, *Rep. Prog. Phys.* **87**, 044502 (2024).
- [6] F. J. Di Salvo, D. E. Moncton, and J. V. Waszquez, Electronic properties and superlattice formation in the semimetal TiSe₂, *Phys. Rev. B* **14**, 4321 (1976).
- [7] D. Wickramaratne, S. Subedi, D. H. Torchinsky, G. Karapetrov, and I. I. Mazin, Photoinduced chiral charge density wave in TiSe₂, *Phys. Rev. B* **105**, 054102 (2022).
- [8] F. X. Bronold, and H. Fehske, Possibility of an excitonic insulator at the semiconductor-semimetal transition, *Phys. Rev. B* **74**, 165107 (2006).
- [9] E. Morosan, H. W. Zandbergen, B. S. Dennis, J. W. G. Bos, Y. Onose, T. Klimczuk, A. P. Ramirez, N. P. Ong, and R. J. Cava, Superconductivity in Cu_xTiSe₂, *Nat. Phys.* **2**, 544 (2006).
- [10] A. F. Kusmartseva, B. Sipos, H. Berger, L. Forró, and E. Tutis, Pressure Induced Superconductivity in Pristine 1T-TiSe₂, *Phys. Rev. Lett.* **103**, 236401 (2009).
- [11] Y. I. Joe, X. M. Chen, P. Ghaemi, K. D. Finkelstein, G. A. de la Peña, Y. Gan, J. C. T. Lee, S. Yuan, J. Geck, G. J. MacDougall, T. C. Chiang, S. L. Cooper, E. Fradkin, and P. Abbamonte, Emergence of charge density wave domain walls above the superconducting dome in 1T-TiSe₂, *Nat. Phys.* **10**, 421 (2014).
- [12] L. J. Li, E. C. T. O'Farrell, K. P. Loh, G. Eda, B. Özyilmaz, and A. H. Castro Neto, Controlling many-body states by the electric-field effect in a two-dimensional material, *Nature* **529**, 185 (2016).
- [13] S.-Y. Xu, Q. Ma, Y. Gao, A. Kogar, A. Zong, A. M. Mier Valdivia, T. H. Dinh, S.-M. Huang, B. Singh, C.-H. Hsu, T.-R. Chang, J. P. C. Ruff, K. Watanabe, T. Taniguchi, H. Lin, G.

- Karapetrov, D. Xiao, P. Jarillo-Herrero, and N. Gedik, Spontaneous gyrotropic electronic order in a transition-metal dichalcogenide, *Nature* **578**, 545 (2020).
- [14] S. Duan, Y. Cheng, W. Xia, Y. Yang, C. Xu, F. Qi, C. Huang, T. Tang, Y. Guo, W. Luo, D. Qian, D. Xiang, J. Zhang, and W. Zhang, Optical manipulation of electronic dimensionality in a quantum material, *Nature* **595**, 239 (2021).
- [15] C. Monney, E. F. Schwier, M. G. Garnier, N. Mariotti, C. Didiot, H. Beck, P. Aebi, H. Cercellier, J. Marcus, C. Battaglia, H. Berger, and A. N. Titov, Temperature-dependent photoemission on 1T-TiSe₂: Interpretation within the exciton condensate phase model, *Phys. Rev. B* **81**, 155104 (2010).
- [16] M. D. Watson, O. J. Clark, F. Mazzola, I. Marković, V. Sunko, T. K. Kim, K. Rossnagel, and P. D. C. King, Orbital- and k_z -selective Hybridization of Se 4*p* and Ti 3*d* States in the Charge Density Wave Phase of TiSe₂, *Phys. Rev. Lett.* **122**, 076404 (2019).
- [17] M. Huber, Y. Lin, G. Marini, L. Moreschini, C. Jozwiak, A. Bostwick, M. Calandra, and A. Lanzara, Ultrafast creation of a light-induced semimetallic state in strongly excited 1T-TiSe₂, *Sci. Adv.* **10**, ead14481 (2024).
- [18] P. Chen, Y. H. Chan, X. Y. Fang, S. K. Mo, Z. Hussain, A. V. Fedorov, M. Y. Chou, and T. C. Chiang, Hidden Order and Dimensional Crossover of the Charge Density Waves in TiSe₂, *Sci. Rep.* **6**, 37910 (2016).
- [19] K. Rossnagel, L. Kipp, and M. Skibowski, Charge-density-wave phase transition in 1T-TiSe₂: Excitonic insulator versus band-type Jahn-Teller mechanism, *Phys. Rev. B* **65**, 235101 (2002).
- [20] S. Koley, M. S. Laad, N. S. Vidhyadhiraja, and A. Taraphder, Preformed excitons, orbital selectivity, and charge density wave order in 1T-TiSe₂, *Phys. Rev. B* **90**, 15146 (2014).
- [21] H. Cercellier, C. Monney, F. Clerc, C. Battaglia, L. Despont, M. G. Garnier, H. Beck, P. Aebi, L. Patthey, H. Berger, and L. Forró, Evidence for an Excitonic Insulator Phase in 1T-TiSe₂, *Phys. Rev. Lett.* **99**, 146403 (2007).
- [22] M. Porer, U. Leierseder, J. M. Ménard, H. Dachraoui, L. Mouchliadis, I. E. Perakis, U. Heinzmann, J. Demsar, K. Rossnagel, and R. Huber, Non-thermal separation of electronic and structural orders in a persisting charge density wave, *Nat. Mater.* **13**, 857 (2014).
- [23] J. van Wezel, P. Nahai-Williamson, and S. S. Saxena, Exciton-phonon-driven charge density wave in TiSe₂, *Phys. Rev. B* **81**, 165109 (2010).
- [24] A. Kogar, M. S. Rak, S. Vig, A. A. Husain, F. Flicker, Y. I. Joe, L. Venema, G. J. MacDougall, T. C. Chiang, E. Fradkin, J. van Wezel, and P. Abbamonte, Signatures of exciton condensation in a transition metal dichalcogenide, *Science* **358**, 1314 (2017).
- [25] Y. Cheng, A. Zong, J. Li, W. Xia, S. Duan, W. Zhao, Y. Li, F. Qi, J. Wu, L. Zhao, P. Zhu, X. Zou, T. Jiang, Y. Guo, L. Yang, D. Qian, W. Zhang, A. Kogar, M. W. Zuerch, D. Xiang, and J. Zhang, Light-induced dimension crossover dictated by excitonic correlations, *Nat. Commun.* **13**, 963 (2022).
- [26] H. Hedayat, C. J. Sayers, D. Bugini, C. Dallera, D. Wolverson, T. Batten, S. Karbassi, S. Friedemann, G. Cerullo, J. van Wezel, S. R. Clark, E. Carpena, and E. D. Como, Excitonic and lattice contributions to the charge density wave in 1T-TiSe₂ revealed by a phonon bottleneck, *Phys. Rev. Res.* **1**, 023029 (2019).
- [27] P. Knowles, B. Yang, T. Muramatsu, O. Moulding, J. Buhot, C. J. Sayers, E. Da Como, and S. Friedemann, Fermi Surface Reconstruction and Electron Dynamics at the Charge-Density-Wave Transition in TiSe₂, *Phys. Rev. Lett.* **124**, 167602 (2020).
- [28] Y. Ou, L. Chen, Z. Xin, Y. Ren, P. Yuan, Z. Wang, Y. Zhu, J. Chen, and Y. Zhang, Incoherence-to-coherence crossover observed in charge-density-wave material 1T-TiSe₂, *Nat. Commun.* **15**, 9202 (2024).
- [29] H. Ueda, M. Porer, J. R. L. Mardegan, S. Parchenko, N. Gurrung, F. Fabrizi, M. Ramakrishnan, L. Boie, M. J. Neugebauer, B. Burganov, M. Burian, S. L. Johnson, K. Rossnagel, and U. Staub, Correlation between electronic and structural orders in 1T-TiSe₂, *Phys. Rev. Res.* **3**, L022003 (2021).
- [30] C. Giannetti, M. Capone, D. Fausti, M. Fabrizio, F. Parmigiani, and D. Mihailovic, Ultrafast optical spectroscopy of strongly correlated materials and high-temperature superconductors: a non-equilibrium approach, *Adv. Phys.* **65**, 58-238 (2016).
- [31] C. Zhang, Q. Wu, W. Hong, H. Liu, S. Zhu, J. Song, Y. Zhao, F. Wu, Z. Liu, S. Liu, Y. Yuan, H. Huang, J. He, S. Li, H. Liu, Y. Duan, H. Luo, and J. Meng, Ultrafast optical spectroscopy evidence of pseudogap and electron-phonon coupling in an iron-based superconductor KCa₂Fe₄As₄F₂, *Sci. China Phys. Mech. Astron.* **65**, 237411 (2022).
- [32] B. L. Tan, C. Zhang, Q. Y. Wu, G. H. Dong, H. Liu, B. Chen, J. J. Song, X. Y. Tian, Y. Zhou, H. Y. Liu, Y. X. Duan, Y. G. Shi, and J. Q. Meng, Anisotropic hybridization dynamics in the quasi-one-dimensional Kondo lattice CeCo₂Ga₈ revealed by ultrafast optical spectroscopy, *Front. Phys.* **20**, 044208 (2025).
- [33] X. F. Tang, S. X. Zhu, H. Liu, C. Zhang, Q. Y. Wu, Z. T. Liu, J. J. Song, X. Guo, Y. S. Wang, H. Ma, Y. Z. Zhao, F. Y. Wu, S. Y. Liu, K. H. Liu, Y. H. Yuan, H. Huang, J. He, W. Xu, H. Y. Liu, Y. X. Duan and J. Q. Meng, Growth, characterization, and Raman spectra of the 1T phases of TiTe₂, TiSe₂, and TiS₂, *Chin. Phys. B* **31**, 037103 (2022).
- [34] C. Monney, M. Puppini, C. W. Nicholson, M. Hoesch, R. T. Chapman, E. Springate, H. Berger, A. Magrez, C. Cacho, R. Ernstorfer, and M. Wolf, Revealing the role of electrons and phonons in the ultrafast recovery of charge density wave correlations in 1T-TiSe₂, *Phys. Rev. B* **94**, 165165 (2016).
- [35] S. X. Zhu, C. Zhang, Q. Y. Wu, X. F. Tang, H. Liu, Z. T. Liu, Y. Luo, J. J. Song, F. Y. Wu, Y. Z. Zhao, S. Y. Liu, T. Le, X. Lu, H. Ma, K. H. Liu, Y. H. Yuan, H. Huang, J. He, H. Y. Liu, Y. X. Duan, and J. Q. Meng, Temperature evolution of quasiparticle dispersion and dynamics in semimetallic 1T-TiTe₂ via high-resolution angle-resolved photoemission spectroscopy and ultrafast optical pump-probe spectroscopy, *Phys. Rev. B* **103**, 115108 (2021).
- [36] Y. M. Dai, J. Bowlan, H. Li, H. Miao, S. F. Wu, W. D. Kong, P. Richard, Y. G. Shi, S. A. Trugman, J. X. Zhu, H. Ding, A. J. Taylor, D. A. Yarotski, and R. P. Prasankumar, Ultrafast carrier dynamics in the large-magnetoresistance material WTe₂, *Phys. Rev. B* **92**, 161104(R) (2015).
- [37] M. Huber, Y. Lin, N. Dale, R. Sailus, S. Tongay, R. A. Kaindl, and A. Lanzara, Revealing the order parameter dynamics of 1T-TiSe₂ following optical excitation, *Sci. Rep.* **12**, 15860 (2022).
- [38] S. Mathias, S. Eich, J. Urbancic, S. Michael, A. V. Carr, S. Emmerich, A. Stange, T. Popmitchchev, T. Rohwer, M. Wiesenmayer, A. Ruffing, S. Jakobs, S. Hellmann, P. Matyba, C. Chen, L. Kipp, M. Bauer, H. C. Kapteyn, H. C. Schneider, K. Rossnagel, M. M. Murnane, and M. Aeschlimann, Self-amplified photo-induced gap quenching in a correlated electron material, *Nat. Commun.* **7**, 12902 (2016).
- [39] S. F. Duan, W. Xia, C. Z. Huang, S. C. Wang, L. X. Gu, H. R. Liu, D. Xiang, D. Qian, Y. F. Guo, and W. T. Zhang, Ultrafast Switching from the Charge Density Wave Phase to a Metastable Metallic State in 1T-TiSe₂, *Phys. Rev. Lett.* **130**, 226501 (2023).
- [40] H. Liu, Q. Y. Wu, C. Zhang, J. Pang, B. Chen, J. J. Song, Y. X. Duan, Y. H. Yuan, H. Y. Liu, C. Shu, Y. F. Xu, Y. G. Shi, and J. Q. Meng, Exploring intrinsic magnetic topological insulators: The case of EuIn₂As₂, *Phys. Rev. B* **110**, 195104 (2024).
- [41] T. Dong, S. J. Zhang, and N. L. Wang, Recent Development of Ultrafast Optical Characterizations for Quantum Materials,

- [Adv. Mater. **35**, 2110068 \(2022\).](#)
- [42] J. A. Holy, K. C. Woo, M. V. Klein, and F. C. Brown, Raman and infrared studies of superlattice formation in TiSe_2 , [Phys. Rev. B **16**, 3628 \(1977\).](#)
- [43] C. S. Snow, J. F. Karpus, S. L. Cooper, T. E. Kidd, and T. C. Chiang, Quantum Melting of the Charge-Density-Wave State in $1T\text{-TiSe}_2$, [Phys. Rev. Lett. **91**, 136402 \(2003\).](#)
- [44] M. Balkanski, R. F. Wallis, and E. Haro, Anharmonic effects in light scattering due to optical phonons in silicon, [Phys. Rev. B **28**, 1928 \(1983\).](#)
- [45] J. Menéndez, and M. Cardona, Temperature dependence of the first-order Raman scattering by phonons in Si, Ge, and $\alpha\text{-Sn}$: Anharmonic effects, [Phys. Rev. B **29**, 2051 \(1984\).](#)
- [46] See Supplemental Material at *** for additional data of $1T\text{-TiSe}_2$.
- [47] W. K. Lee, H. Z. Cummins, R. M. Pick, and C. Dreyfus, Amplitude mode in K_2SeO_4 : Temperature dependence of the Raman cross section, [Phys. Rev. B **37**, 6442 \(1988\).](#)
- [48] L. Cui, R. He, G. Li, Y. Zhang, Y. You, and M. Huang, Raman spectroscopy of optical phonon and charge density wave modes in $1T\text{-TiSe}_2$ exfoliated flakes, [Solid State Commun. **266**, 21 \(2017\).](#)
- [49] L. Stojchevska, I. Vaskivskiy, T. Mertelj, P. Kusar, D. Svetin, S. Brazovskii, and D. Mihailovic, Ultrafast switching to a stable hidden quantum state in an electronic crystal. [Science **344**, 177 \(2014\)](#)
- [50] Z. T. Liu, C. Zhang, Q. Y. Wu, H. Liu, B. Chen, Z. B. Yin, S. T. Cui, Z. Sun, S. X. Zhu, J. J. Song, Y. Z. Zhao, H. Y. Zhang, X. Q. Ye, F. Y. Wu, S. Y. Liu, X. F. Tang, Y. H. Yuan, Y. P. Wang, J. He, H. Y. Liu, Y. X. Duan, and J. Q. Meng, Charge density wave order and electron-boson coupling in ternary superconductor $\text{Bi}_2\text{Rh}_3\text{Se}_2$, [Sci. Chin-Phys. Mech. Astron. **66**, 277411 \(2023\).](#)
- [51] Q. Y. Wu, C. Zhang, B. Z. Li, H. Liu, J. J. Song, B. Chen, H. Y. Liu, Y. X. Duan, J. He, J. Liu, G. H. Cao, J. Q. Meng, Interplay of electron-phonon coupling, pseudogap, and superconductivity in $\text{CsCa}_2\text{Fe}_4\text{As}_4\text{F}_2$ studied using ultrafast optical spectroscopy, [Phys. Rev. B **111**, L081110 \(2025\).](#)
- [52] K. Ishioka, M. Hase, M. Kitajima, L. Wirtz, A. Rubio, and H. Petek, Ultrafast electron-phonon decoupling in graphite, [Phys. Rev. B **77**, 121402 \(2008\).](#)